The Second Generation (G2) Fingertip Sensor for Near-Distance Ranging and Material Sensing in Robotic Grasping*

Cheng Fang, Di Wang, Dezhen Song, and Jun Zou

Abstract— **To continuously improve robotic grasping, we are interested in developing a contactless fingertip-mounted sensor for near-distance ranging and material sensing. Previously, we demonstrated a dual-modal and dual sensing mechanisms (DMDSM) pretouch sensor prototype based on pulse-echo ultrasound and optoacoustics. However, the complex system, the bulky and expensive pulser-receiver, and the omni-directionally sensitive microphone block the sensor from practical applications in real robotic fingers. To address these issues, we report the second generation (G2) DMDSM sensor without the pulser-receiver and microphone, which is made possible by redesigning the ultrasound transmitter and receiver to gain much wider acoustic bandwidth. To verify our design, a prototype of the G2 DMDSM sensor has been fabricated and tested. The testing results show that the G2 DMDSM sensor can achieve better ranging and similar material/structure sensing performance, but with much-simplified configuration and operation. The primary results indicate that the G2 DMDSM sensor could provide a promising solution for fingertip pretouch sensing in robotic grasping.**

I. Introduction and Related Work

Robust grasping of unknown objects is a grand challenge in robotics [1] [2]. When robots move from industry floors to a wide range of domestic applications, the prior knowledge of targeted objects is often not available which makes it impossible to use sensor-less grasping [3] [4]. Sensor-based approaches are expected to provide object relative pose and material/structure information. Ideally, assisted by the near-distance (e.g. < 0.5 cm) ranging, robotic fingers can adjust grasping plan dynamically by responding to subtle changes in object pose right before the grasping contact. Moreover, sensors should provide the material-type and interior structure information which can help planner better anticipate the force distribution, impact characteristics, and friction coefficients to form a more robust grasping plan. Unfortunately, to a large degree, current sensors cannot satisfy these requirements. Existing sensors, such as cameras and laser range finders, suffer from the occlusion caused by closing-in robotic grippers [5] or having a near-range blind zone [6] [7] [8] [9]. Tactile [10] [11] and force sensors [12] require physical contact with the target object. The contact may change object poses, damage the grasping target, or lead to slow grasping or a complete failure. Therefore, a contactless sensing solution is more desirable. Recent development of proximity/pre-touch sensors based on optical, electric-field, and ultrasound signals have made great progress, but still suffer from significant limitations from their sensing modalities and/or limited target materials. For example, electric-field sensors are challenged by targets with dielectric constants close to that of air [13] [14] [15] [16]. Optical pre-touch sensors lack lateral resolution and cannot handle optically-transparent or highly-reflective targets [17] [18] [19] [20]. Ultrasound-based sensors fail on sound absorbing or reflective materials [21] [22] [23] [24].

Previously, we demonstrated a dual-modal and dual sensing mechanisms (DMDSM) pretouch sensor for both near-distance ranging and material/interior structure sensing based on pulse-echo ultrasound and optoacoustics [25]. Pulse-echo ultrasound utilizes the transmitted and reflected acoustic signals to interrogate target distance and material/structure. Optoacoustics relies on the optoacoustic signals directly generated from the target upon laser excitation. In both modalities, the temporal delay of signals is used to determine the target-sensor distance for ranging, while their frequency spectra are used to extract distinctive features for classifying the target materials or (inner) structures. Although the DMDSM sensor worked well as a prototype for the initial demonstration, several issues still remain in its design and operation, which could limit its performance and functionalities in real grasping applications (Fig. 1(a)). First, it consists of two transmitters and two receivers for handling the low- and high-frequency acoustic signals, respectively, which make the sensor construction and more importantly, the operation rather complex. Second, as the low-frequency acoustic receiver, the microphone has a wide reception angle and is sensitive to ambient noise in the surrounding environment. Although the environmental noise may be canceled by adding a second microphone, it will make the DMDSM sensor even more complex. Third, the pulser-receiver generates high-voltage electric pulses, which could make the DMDSM sensor unsafe to work in flammable or explosive environments. In addition, one pulser-receiver unit, which is bulky and expensive, can only interface with one DMDSM sensor, making it impractical to build and operate multiple sensors simultaneously.

To address these issues, we report the second generation (G2) DMDSM sensor with a much-simplified design and operation procedure (Fig. 1(b)). As the major innovations, both the ultrasound transmitter and receiver are redesigned to significantly improve their acoustic bandwidth for the excitation (upon laser pulse illumination) and reception of both low- and high-frequency acoustic signals. As a result, both ranging and material/structure sensing can be achieved with a single transmitter and receiver, and also makes the microphone and pulser-receiver unnecessary. For

*The research is supported in part by National Science Foundation under NRI-1925037.

C. Fang and J. Zou are with the Electrical and Computer Engineering Department, Texas A&M University, College Station, TX 77843, USA (e-mails: {fangchengok2007, junzou}@tamu.edu).

D. Wang and D. Song are with the Computer Science and Engineering Department, Texas A&M University, College Station, TX 77843, USA (e-mails: ivanwang@tamu.edu, dzsong@cs.tamu.edu).

demonstration, a prototype G2 DMDSM sensor is designed, fabricated, and tested. The testing results show that the G2 DMDSM sensor can achieve better ranging and similar material/structure sensing performances compared with the G1 sensor [25] (and older designs [26] [27]), but with reduced complexity, simpler operation, and higher resistance to environmental noise.

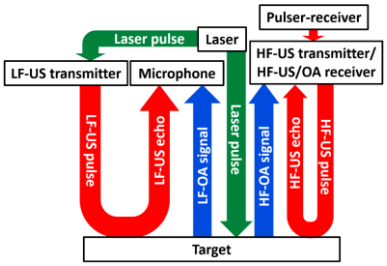

(a)

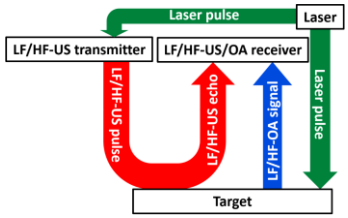

(b)

Figure 1. The flow charts showing the working principles of (a) G1 and (b) G2 DMDSM sensors. HF: high-frequency; LF: low-frequency; US: ultrasound; OA: optoacoustic. Best viewed in color.

II. Sensor Design, Construction and Testing

Figure 2 shows the schematic design of the G2 DMDSM sensor. Different from the G1 sensor with two transmitters and two receivers, it consists of only one ultrasound transmitter and one receiver in a co-centered and co-axial configuration. Driven by collimated pulsed laser beams, the transmitter sends both low- and high-frequency ultrasound pulses to the target (after being reflected and focused by the parabolic mirror). The echo signals travelling back along the reverse path are collected by a ring-shaped transducer as the receiver. Pulse-echo ranging and material/structure sensing are conducted based on the time delays and frequency spectra of the collected echo signals, respectively. Because the transmitter is driven solely by the laser pulses, the pulser-receiver used in the G1 sensor now becomes unnecessary. For optoacoustic ranging/sensing, the inner part of the pulsed laser beam passes through the center hole of the ultrasound transmitter and is incident onto the target surface (after being reflected and focused by the parabolic mirror). The excited optoacoustic signals are also collected by the ring-shaped transducer. Their time delays and frequency spectra are used for optoacoustic ranging and material/structure sensing, respectively.

For the G2 DMDSM sensor, one laser pulse will trigger the collection of both pulse-echo ultrasound and optoacoustic signals by the same receiver, which greatly simplifies the sensor operation and data acquisition. It should be noted that this single triggering data acquisition scheme will not cause the mixing of pulse-echo ultrasound and optoacoustic signals. This is because pulse-echo signal goes through a round trip (transmitter–target–receiver) with a time delay twice that of the optoacoustic signal after a single trip (target–receiver), and the difference in their time delays is much longer than their durations, resulting in clear separation in the time domain.

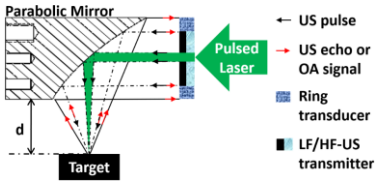

Figure 2. Schematic design of the G2 DMDSM sensor. HF: high-frequency; LF: low-frequency; US: ultrasound; OA: optoacoustic.

Without using pulser-receiver, both low- and high-frequency ultrasound signals for pulse-echo ultrasound ranging and sensing have to be generated by the optoacoustic ultrasound transmitter. In the G1 DMDSM sensor, the optoacoustic ultrasound transmitter has a transmission bandwidth of 0–90 kHz (from the flexural-mode vibration), which was designed to match the reception bandwidth of microphone (0–80 kHz). However, such low frequencies cannot provide high ranging resolution. To address this issue, the optoacoustic ultrasound transmitter is redesigned (Fig. 3). It consists of an optically-transparent acrylic supporting substrate and a layer of black vinyl electrical tape as the laser absorption layer. Both acrylic and vinyl have low Young's modulus (~GPa) and high internal damping, which allows effective generation of wideband ultrasound signals from low-frequency (~kHz) flexural and high-frequency (~MHz) thickness modes. The acrylic substrate has a thickness of 1.6 mm and a diameter of 9 mm. A center hole with a diameter of 1.5 mm is opened to allow the pulsed laser to pass through for optoacoustic ranging and material/structure sensing.

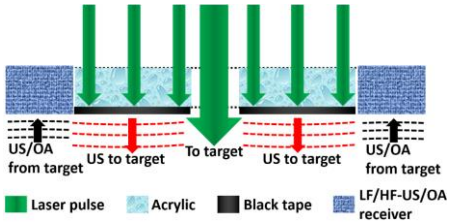

Figure 3. A zoom-in diagram of the redesigned optoacoustic ultrasound transmitter and ring PZT transducer under pulsed laser illumination. They form a co-centered and co-axial arrangement. HF: high-frequency; LF: low-frequency; US: ultrasound; OA: optoacoustic.

Distinctive features about the material properties and sub-surface structures are more carried by the lower-frequency components of the acoustic spectra (up to 10s of kHz) [28] [29] [30] [31]. However, the previous ring PZT (lead zirconate titanate) transducer typically operates at much higher MHz frequencies with a narrow bandwidth, which cannot effectively capture the low-frequency acoustic spectra needed for the target material/structure sensing. To address this issue, the ring PZT transducer is also redesigned to receive both low- and high-frequency acoustic signals for ranging and material/structure sensing. First, a thicker backing layer of epoxy is added to better damp the acoustic resonance of the PZT layer. Second, the inner diameter of the ring transducer is increased to induce multiple modes of

vibration, e.g., radial (~kHz) and thickness modes (~MHz). With the above two improvements, the bandwidth of the redesigned ring PZT transducer is widened to better match that of the optoacoustic ultrasound transmitter.

The collective bandwidth of the redesigned optoacoustic ultrasound transmitter and ring PZT transducer is characterized (Fig. 4(a)). A Q-switched 532nm Nd:YAG pulsed laser is used as the light source with a repetition rate of 10 Hz, a pulse duration of 8 ns, and an average pulse energy around 2.5 mJ/pulse. The laser beam is firstly expanded by two lenses and then filtered by an iris with $\phi \sim 9$ mm to illuminate the black tape layer in the optoacoustic ultrasound transmitter. The distance between the ring PZT transducer and the optoacoustic ultrasound transmitter is around 2 cm. A photo detector is used to detect the laser pulse and generate a trigger signal to synchronize the data acquisition. The received signals are amplified by a preamplifier and recorded by an oscilloscope. A representative waveform and its frequency spectrum received by the ring PZT transducer are shown in Figs. 4(b) and 4(c), respectively. The time-domain waveform consists of two pulses due to the multiple reflection between the transmitter and ring PZT transducer. The acoustic frequency spectrum indicates the collective bandwidth of the redesigned transmitter and ring PZT transducer with center frequencies around 80 kHz, 532 kHz, and 728 kHz. The wideband response is superior to that of the G1 sensor, consisting of two isolated bands at 0–90 kHz and 1–2 MHz.

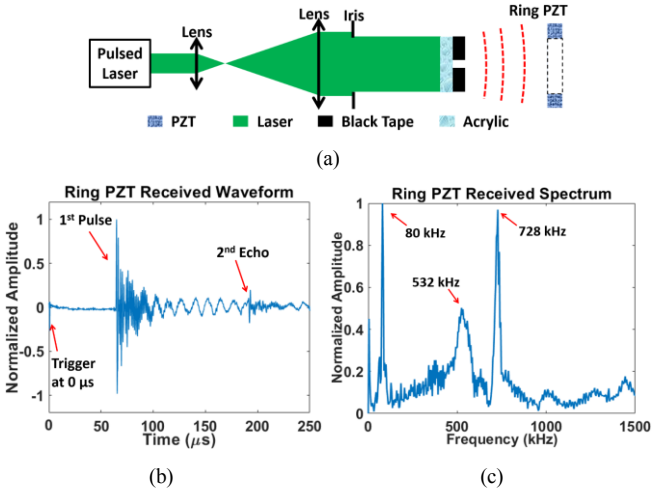

Figure 4. (a) Diagram of the setup to characterize the collective bandwidth of the redesigned ultrasound transmitter and ring PZT transducer. Representative (b) waveform and (c) frequency spectrum of the received ultrasound signals.

Fig. 5(a) shows the fabricated prototype of the G2 DMDSM sensor (weight ~ 20 grams), consisting of a 3D-printed housing (66.4 mm × 27.8 mm × 24.2 mm), a 90-degree parabolic mirror, the redesigned wideband ultrasound transmitter, and ring PZT transducer. A testing setup is built to characterize the pulse-echo ultrasound and optoacoustic ranging and sensing performances of the G2 DMDSM sensor (Fig. 2). The same pulsed laser in setup Fig. 4(a) is used as the light source for optoacoustic excitation. One laser pulse initiates simultaneous optoacoustic and pulse-echo ultrasound data acquisition. The optoacoustic and ultrasound signals received by the ring PZT transducer are amplified by a preamplifier and then recorded by an oscilloscope (Fig. 5(b), 250-μs data duration). The time delays of the 1st optoacoustic signal, the pulse-echo ultrasound signal, and the 2nd optoacoustic signal (echo after a round trip) are around 75 μs, 150 μs, and 225 μs, respectively, which are long enough for isolating the real optoacoustic/ultrasound signals from other unwanted signals for ranging/sensing.

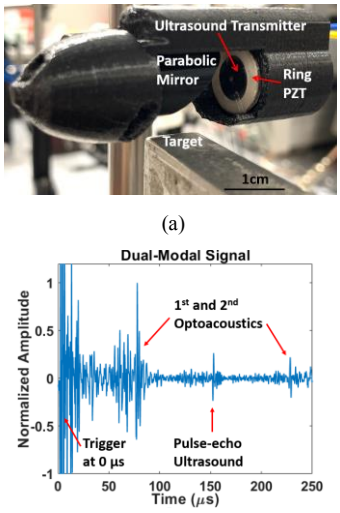

Figure 5. (a) Photograph of a fabricated protoype of the G2 DMDSM sensor. (b) Representative waveform of the received optoacoustic and pulse-echo ultrasound signals from a 6.35-mm-thick aluminum target through air.

III. Ranging Experiment and Results

A. *Pulse-echo Ultrasound Distance Ranging*

For pulse-echo ultrasound distance ranging, a piece of 1-mm-thickness glass slide is firstly used as the target. The distance (d) between the parabolic mirror and the glass slide is decreased from 11.0 mm to 0.5 mm with a decrement of 0.5 mm. The measured distance vs. the real distance (d) and their deviations are shown in Figs. 6(a) and 6(b), respectively. The deviation is smaller than 0.3 mm within the ultrasound focal zone where d is between 4.0 mm and 7.0 mm. The same setup is used to quantify the lateral resolution of the pulse-echo ultrasound ranging, except that the glass slide target is replaced by a copper wire with a diameter around 0.7 mm. After repeating the lateral scan at different distance (d) from 3.5 mm to 7.5 mm, the ultrasound lateral resolution is determined by the minimal acoustic focal diameter (Fig. 6(c)), indicating the lateral resolution around 0.60 mm at the focal length d = 5.5 mm. The measured depth of focus (DOF) is also around 3.0 mm where d changes from 4.0 mm to 7.0 mm.

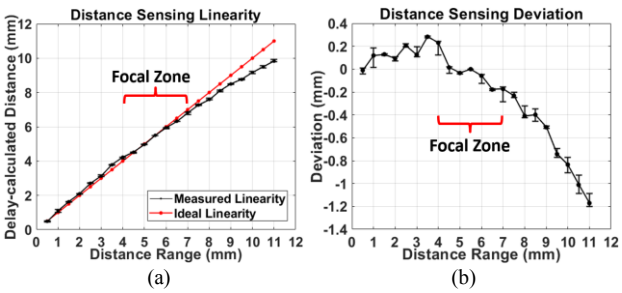

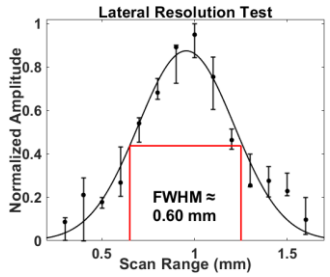

(c)

Figure 6. (a) Comparison between measured (in black) and real (in red) distances. (b) Deviation of the measured distance from the real distance. (c) Pulse-echo ultrasound lateral resolution of 0.60 mm determined by the minimal acoustic focal diameter at d=5.5 mm.

B. Optoacoustic Distance Ranging

The optoacoustic distance ranging is characterized with a 0.1-mm-diameter copper wire as the target. The distance (d) between the parabolic mirror and the target is decreased from 7 mm to 5 mm with a decrement of 0.5 mm. The measured distance vs. the real distance (d) and their deviations are shown in Figs. 7(a) and 7(b), respectively. The deviation is smaller than 0.2 mm within the optoacoustic focal zone where d is between 5.5 mm and 6.5 mm. The same setup is used to quantify the optoacoustic lateral resolution, where the same copper wire is scanned laterally. After repeating the lateral scan at different distance (d) from 5.0 mm to 7.0 mm, the optoacoustic lateral resolution is determined by the minimal optoacoustic focal diameter (Fig. 7(c)), indicating a lateral resolution ~61.7 μm at the focal point (d = 6.0 mm). The measured DOF is also around 1.0 mm where d changes from 5.5 mm to 6.5 mm.

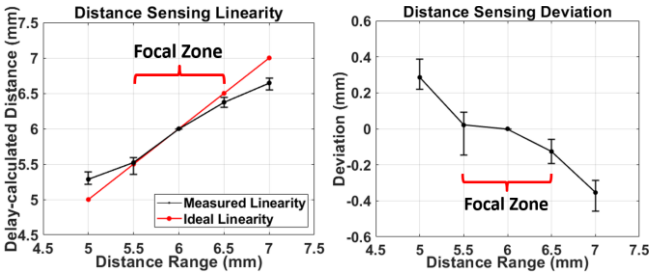

(a) (b)

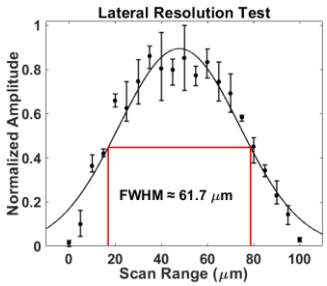

(c)

Figure 7. (a) Comparison between the measured (in black) and the real (in red) distances. (b) Deviation of the measured distance from the real distance. (c) Optoacoustic lateral resolution of 61.7 μm determined by the minimal optoacoustic focal diameter at d = 6.0 mm.

Table 1 lists and compares the distance ranging performances of the G1 and G2 DMDSM sensors. For pulse-echo ultrasound ranging, both the working range (i.e., DOF) and the lateral resolution are improved. This is because the redesigned optoacoustic ultrasound transmitter has a fuller aperture than the previous transmitter (i.e., the ring PZT transducer), which provides higher beam quality for acoustic transmission. Also, the maximum deviation within the DOF is slightly increased, possibly due to slightly lower detection frequency of the ring PZT transducer. For optoacoustic ranging, the working range (i.e., DOF) remains the same, while the lateral resolution is somewhat improved. This is mainly due to the reduced laser pulse energy (~70 μJ vs. ~560 μJ for the G1 sensor setup [25]). As a result, the amplitude of the optoacoustic signal becomes more sensitive to the lateral scanning position. On the other hand, the reduced laser pulse energy and lower detection frequency of the ring PZT transducer contribute to the slightly larger maximum deviation within the DOF.

TABLE I. THE RANGING PERFORMANCES COMPARISION OF THE G1 AND G2 DMDSM SENSORS

Ranging Performances	G1 Sensor [25]	G2 Sensor
Pulse-echo Max Deviation	0.24 mm	0.29 mm
Pulse-echo DOF	2.0 mm	**3.0 mm**
Pulse-echo Lateral Resolution	1.04 mm	**0.60 mm**
Optoacoustic Max Deviation	0.12 mm	0.20 mm
Optoacoustic DOF	1.0 mm	1.0 mm
Optoacoustic Lateral Resolution	95.0 μm	**61.7 μm**

IV. MATERIAL SENSING EXPERIMENT AND RESULTS

A. Data Acquisition and Classification

Both the low- and high-frequency components of the optoacoustic and ultrasound echo signals received by the ring PZT transducer are used for material / sub-surface structure (especially the thickness) sensing. Depending on the optical and mechanical properties of the target, the received signals mainly consist of either target-induced optoacoustic signal, or target-reflected ultrasound echo signal, or both. This kind of DMDSM signals is expected to provide more distinctive features for the material/structure sensing. The material/structure differentiation has been performed with the same Bag-of-SFA-Symbols (BOSS) classifier [32] [33]. The classifier is trained to identify the different material/structure, where the original data set is randomly divided into the training and testing data with 3:1 ratio without overlapping. The experimental data are transformed into BOSS histograms, serving as feature set for classification. After 50 random trials, the BOSS classifier gives the confusion matrix to show the accuracy of classification.

B. Material/Thickness Differentiation

To compare the performance of the G2 DMDSM sensor with that of the G1 sensor, the same group of targets, including acrylic, aluminum block, paper, rubber, steel, and also aluminum sheets with different thickness are used for material/sub-surface structure (thickness) differentiation. The captured waveforms, including the optoacoustic and / or ultrasound signals, are similar as Fig. 5(b), which carry the distinctive features about the material properties and sub-surface structures. The representative DMDSM acoustic spectra are shown in Figs. 8 and 9. The confusion matrices given by BOSS classifier (Fig. 10) indicate ≥98.0% overall accuracy of the material differentiation and ≥99.5% overall

accuracy of the thickness classification, which are similar with those obtained with the G1 sensor [25].

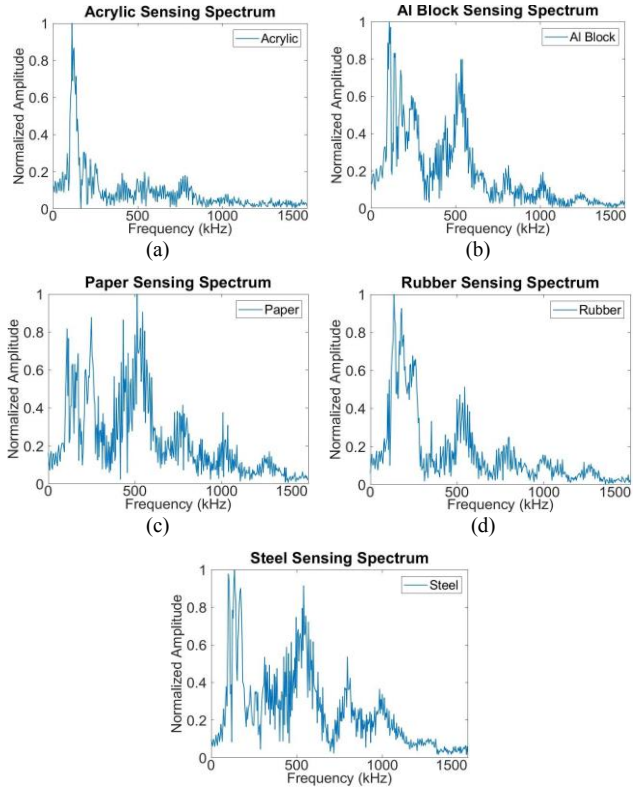

Figure 8. Representative DMDSM acoustic spectra from (a) acrylic, (b) aluminum block, (c) paper, (d) rubber, and (e) steel.

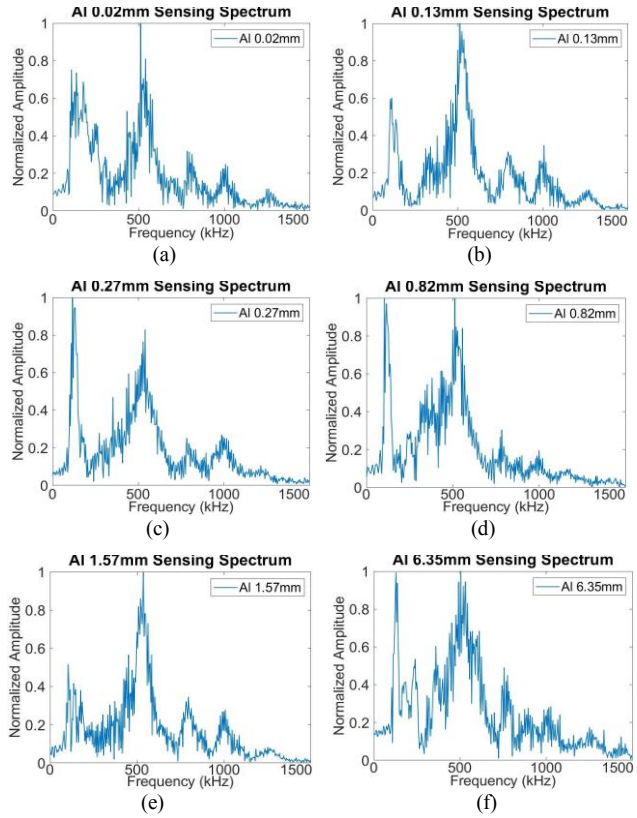

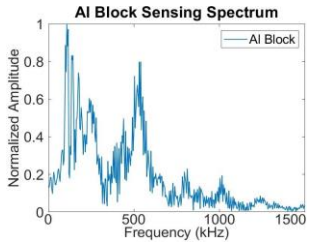

(g)

Figure 9. Representative DMDSM acoustic spectra from aluminum sheets with different thickness.

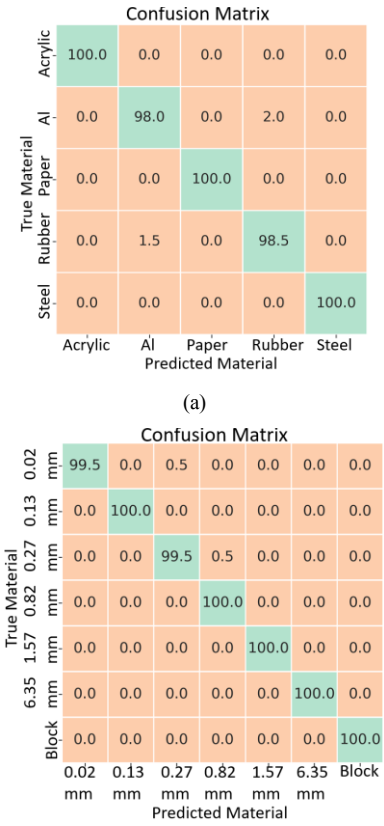

Figure 10. BOSS classifier averaged confusion matrix of (a) different materials and (b) aluminum sheets with different thickness.

C. Differentiation of Challenging Targets

To further investigate the material sensing capabilities of the G2 DMDSM sensor, the same eight optical and acoustic challenging targets (OACTs) once used to characterize the G1 sensor [25] are tested (Fig. 11), including four optically-transparent targets of glass, acrylic, PET (polyethylene terephthalate), PDMS (polydimethylsiloxane) (Figs. 11(a)-(d)) with low optoacoustic generation efficiency, and four dark thin/porous targets of fabric, foam, paper, window tint film (Figs. 11(e)-(h)) with weak acoustic reflection. To compensate the target thickness difference, the height of Z-axis stage is adjusted until the target top is at the focus of the parabolic mirror (Fig. 2). The representative DMDSM acoustic spectra from the eight targets are shown in Fig. 12. BOSS classifier gives the confusion matrix showing a 97% overall accuracy for all the targets (Fig. 13), which are also similar with those obtained with the G1 sensor [25].

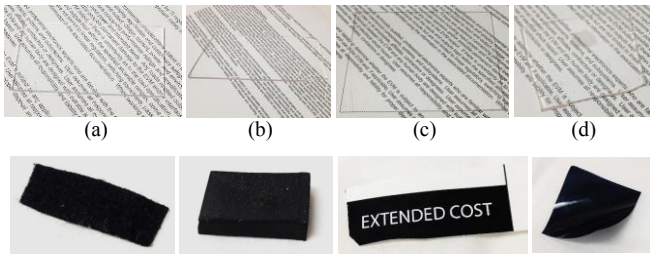

Figure 11. Photos of the eight OACTs: (a)–(d) optically-transparent targets of glass, acrylic, PET (with contour marked by dash line), PDMS with thicknesses around 1.0 mm, 1.6 mm, 0.11 mm, and 1.5 mm separately, and (e)–(h) dark thin/porous targets of fabric, foam, paper, window tint film with thicknesses around 2 mm, 8 mm, 0.1 mm, 0.06 mm separately.

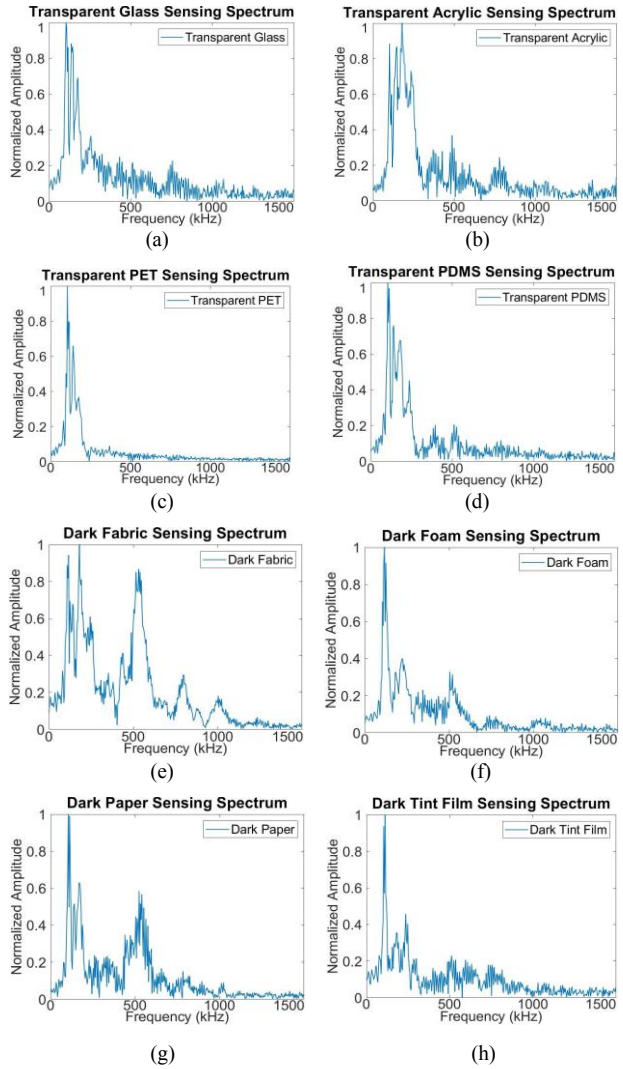

Figure 12. Representative DMDSM acoustic spectra from (a)–(d) optically-transparent targets and (e)–(h) dark thin/porous targets.

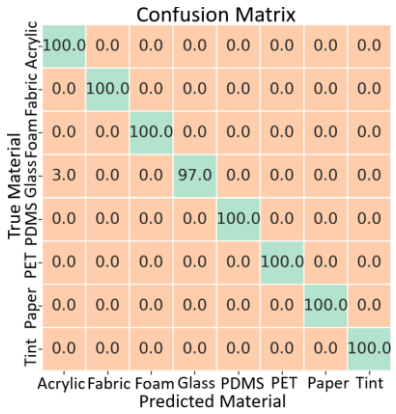

Figure 13. BOSS classifier averaged confusion matrix of the eight OACTs.

V. Conclusion and Future Work

In this paper, we demonstrate the second-generation (G2) fingertip-mounted DMDSM sensor for near-distance pulse-echo ultrasound and optoacoustic ranging and material/structure sensing for robotic grasping. The G2 DMDSM sensor is much simpler and easier to operate than the G1 sensor, while providing improved ranging and similar sensing performances. These improvements make it much more practical to be used on a robotic hand for facilitating the grasping. Before mounting the sensor on a robotic hand, some additional work needs to be completed. First, as Table I, the OA and US working range (DOF) is relatively limited, which is expected to be enlarged for more flexible moving and vibration of the robotic finger. Second, laser pulses were directly delivered from a relatively bulky laser head in current setup, which is expected to be replaced by optical fibers from a portable light source.

In the future, we plan to solve these challenges as well as test more materials and sub-surface structures to optimize the ranging and sensing performance. After that, we will integrate the sensor onto robot fingers to characterize its performance, develop perception algorithms, and enable real time close-loop grasping.

Acknowledgment

The authors would like to thank for the inputs and feedback from Xiaoyu Duan and Fengzhi Guo.

References

[1] M. T. Mason, Mechanics of Robotic Manipulation, MIT press, 2001.

[2] M. Ciocarlie, K. Hsiao, E.G. Jones, S. Chitta, R.B. Rusu and I.A. Şucan, "Towards reliable grasping and manipulation in household environments," *Experimental Robotics,* pp. 241-252, Springer, Berlin, Heidelberg, 2014.

[3] K. Y. Goldberg, "Orienting Polygonal Parts Without Sensors," *Algorithmica,* vol. 10, no. 2-4, pp. 201-225, 1993.

[4] M. A. Erdmann and M. T. Mason, "An exploration of sensorless manipulation," *IEEE Journal on Robotics and Automation,* vol. 4, no. 4, pp. 369-379, 1988.

[5] C. E. Smith and N. P. Papanikolopoulos, "Vision-Guided Robotic Grasping: Issues and Experiments," *Proceedings of IEEE International Conference on Robotics and Automation,* vol. 4, pp. 3203-3208, 1996.

[6] A. Wehr and U. Lohr, "Airborne laser scanning—an introduction and overview," *ISPRS Journal of photogrammetry and remote sensing,* vol. 54, no. 2-3, pp. 68-82, 1999.

[7] Y. Lu, J. Lee, S. H. Yeh, H. M. Cheng, B. Chen and D. Song, "Sharing Heterogeneous Spatial Knowledge: Map Fusion between Asynchronous Monocular Vision and Lidar or Other Prior Inputs," *Robotics Research,* pp. 727-741, Springer, Cham, 2020.

[8] M. C. Amann, T. M. Bosch, M. Lescure, R. A. Myllylae and M. Rioux, "Laser ranging: a critical review of unusual techniques for distance measurement," *OptEn,* vol. 40, pp. 10-19, 2001.

[9] A. Stelzer, M. Jahn and S. Scheiblhofer, "Precise distance measurement with cooperative FMCW radar units," *2008 IEEE Radio and Wireless Symposium,* pp. 771-774, 2008.

[10] R. D. Howe, "Tactile sensing and control of robotic manipulation," *Advanced Robotics,* vol. 8, no. 3, pp. 245-261, 1993.

[11] J. M. Romano, K. Hsiao, G. Niemeyer, S. Chitta and K. J. Kuchenbecker, "Human-Inspired Robotic Grasp Control With Tactile Sensing," *IEEE Transactions on Robotics,* vol. 27, no. 6, pp. 1067-1079, 2011.

[12] Q. Xu, "Design and Development of a Novel Compliant Gripper With Integrated Position and Grasping/Interaction Force Sensing," *IEEE Transactions on Automation Science and Engineering,* vol. 14, no. 3, pp. 1415 - 1428, 2015.

[13] J. R. Smith, E. Garcia, R. Wistort and G. Krishnamoorthy, "Electric field imaging pretouch for robotic graspers," *2007 IEEE/RSJ International Conference on Intelligent Robots and Systems,* pp. 676-683, 2007.

[14] R. Wistort and J. R. Smith, "Electric field servoing for robotic manipulation," *In 2008 IEEE/RSJ International Conference on Intelligent Robots and Systems,* pp. 494-499, 2008, September.

[15] B. Mayton, L. LeGrand and J. R. Smith, "An electric field pretouch system for grasping and co-manipulation," *2010 IEEE International Conference on Robotics and Automation,* pp. 831-838, 2010.

[16] B. Mayton, E. Garcia, L. LeGrand and J. R. Smith, "Electric field pretouch: Towards mobile manipulation," *In RSS Workshop on Mobile Manipulation in Human Environments,* 2009, June.

[17] K. Hsiao, P. Nangeroni, M. Huber, A. Saxena and A. Y. Ng, "Reactive grasping using optical proximity sensors," *2009 IEEE International Conference on Robotics and Automation,* pp. 2098-2105, 2009.

[18] B. Yang, P. Lancaster and J. R. Smith, "Pre-touch sensing for sequential manipulation," *2017 IEEE International Conference on Robotics and Automation (ICRA),* pp. 5088-5095, 2017.

[19] H. Hasegawa, Y. Mizoguchi, K. Tadakuma, A. Ming, M. Ishikawa and M. Shimojo, "Development of intelligent robot hand using proximity, contact and slip sensing," *In 2010 IEEE International Conference on Robotics and Automation,* pp. 777-784, 2010, May.

[20] A. Maldonado, H. Alvarez and M. Beetz, "Improving robot manipulation through fingertip," *In 2012 IEEE/RSJ International Conference on Intelligent Robots and Systems,* pp. 2947-2954, 2012.

[21] L. Jiang and J. R. Smith, "A unified framework for grasping and shape acquisition via pretouch sensing," *In 2013 IEEE International Conference on Robotics and Automation,* pp. 999-1005, 2013, May.

[22] E. Guglielmelli, V. Genovese, P. Dario and G. Morana, "Avoiding obstacles by using a proximity us/ir sensitive skin," *In Proceedings of 1993 IEEE/RSJ International Conference on Intelligent Robots and Systems (IROS'93),* vol. 3, pp. 2207-2214, 1993, July.

[23] L. Jiang and J. R. Smith, "Seashell effect pretouch sensing for robotic grasping," *In 2012 IEEE International Conference on Robotics and Automation,* pp. 2851-2858, 2012, May.

[24] L. T. Jiang and J. R. Smith, "Pretouch sensing for manipulation," *In Robotics: Science and Systems (RSS) Workshop: Alternative Sensing Techniques for Robotic Perception,* 2012, July.

[25] C. Fang, D. Wang, D. Song and J. Zou, "Fingertip Pulse-Echo Ultrasound and Optoacoustic Dual-Modal and Dual Sensing Mechanisms Near-Distance Sensor for Ranging and Material Sensing in Robotic Grasping," *IEEE International Conference on Robotics and Automation (ICRA) (Accepted),* 2021.

[26] C. Fang, D. Wang, D. Song and J. Zou, "Toward Fingertip Non-Contact Material Recognition and Near-Distance Ranging for Robotic Grasping," *2019 IEEE International Conference on Robotics and Automation (ICRA),* pp. 4967-4974, 2019.

[27] C. Fang, D. Wang, D. Song and J. Zou, "Fingertip Non-Contact Optoacoustic Sensor for Near-Distance Ranging and Thickness Differentiation for Robotic Grasping," *2020 IEEE/RSJ International Conference on Intelligent Robots and Systems (IROS),* pp. 10894-10899, IEEE, 2020.

[28] I. P. Dunn and W. A. Davern, "Calculation of acoustic impedance of multi-layer absorbers," *Applied acoustics,* vol. 19, no. 5, pp. 321-334, 1986.

[29] M. E. Delany and E. N. Bazley, "Acoustical Properties of Fibrous Absorbent Materials," *Applied acoustics= Acoustique appliqu = Angewandte Akustik,* vol. 3, no. 2, pp. 105-116, 1970.

[30] M. I. Khan and G. J. Diebold, "The photoacoustic effect generated by laser irradiation of an isotropic solid cylinder," *Ultrasonics,* vol. 34, no. 1, pp. 19-24, 1996.

[31] R. D. Mindlin and H. Deresiewicz, "Thickness-shear and flexural vibrations of a circular disk," *Journal of applied physics,* vol. 25, no. 10, pp. 1329-1332, 1954.

[32] P. Schäfer, "The BOSS is concerned with time series classification in the presence of noise," *Data Mining and Knowledge Discovery,* vol. 29, no. 6, pp. 1505-1530, 2015.

[33] A. Bagnall, J. Lines, A. Bostrom, J. Large and E. Keogh, "The great time series classification bake off: a review and experimental evaluation of recent algorithmic advances," *Data Mining and Knowledge Discovery,* vol. 31, no. 3, pp. 606-660, 2017.